MIST-ASSISTED FILM COOLING TECHNIQUE FOR TURBINE BLADE LEADING EDGE

Ajay Kumar Jaiswal, Pallab Sinha Mahapatra*

Department of Mechanical Engineering, Indian Institute of Technology Madras, Chennai 600042, India

ABSTRACT

In this computational work, the advantages of mist-assisted film cooling have been demonstrated over air film cooling. For this, a semi-circular body approximating the blade's leading edge was considered with five rows of film holes, each having five holes. All film holes were arranged in a staggered manner with injection angles of 0^0, $\pm 25^0$ and $\pm 50^0$. The ANSYS Fluent 18.1 version was used to do steady-state simulations with the $SST\ k-\omega$ turbulence model. The effect of droplets diameter was also investigated for a constant mass flow rate of coolant. The effectiveness enhancement was observed by adding 2% mist particle (on a mass basis) and droplet size of $d_p = 5, 10\ and\ 15 \mu m$. The effectiveness was found to diminish with an increase of droplets diameter. At the unity blowing ratio, the increase in area-weighted averaged effectiveness was determined to be $\sim 32\%$.

1. INTRODUCTION

An efficient cooling strategy for the turbine vane/blade is critical to keep the construction material within safe working limits in the current gas turbine industry. For the past few decades, many cooling methods such as jet impingement, convection cooling, and film cooling have been deployed. The first two methods are internal cooling, whereas the film cooling, is external cooling strategy. During film cooling the coolant ejected from discrete film holes forms a protective coating of coolant near the blade's outer surface, shielding the blade material from hot flue gas [1]. Mist particle/water droplets can be introduced to the coolant to enhance cooling effectiveness. Water droplets act as a discrete heat sink by absorbing heat during evaporation, enabling heated mainstream gases to cool even faster. The film cooling efficiency improves due to the significantly cooler air, which cools the material to a greater extent. Mist cooling effectiveness is influenced by the size of the droplets, the percentage of mist, and the temperature.

Nirmalan et al. [2] claiming a 50% reduction in coolant supply while using a mist-assisted film cooling approach for turbine vanes. Li and Wang's computational research [3] looked at droplet size and mist proportion effects. They concluded that smaller droplets may be more efficient at high mist flow rates than larger droplets. Under real-world gas turbine operating conditions, In a laboratory setting, Zhao and Wang [4] investigated the adiabatic film cooling efficacy and coverage of mist-assisted air film cooling and air film cooling. They discovered that the cooling air-droplet combination does not always match the droplet layer and that with a high blowing ratio, around 17% of the droplets migrate outside the film. As a result, film cooling effectiveness decreases, followed by a rising tendency. This happens at the "bending back" point of the mist film. As the mist-air mixture is injected, the coolant jet rises and bends back. This means that as the mist film bends back and approaches the surface, the surface temperature drops, increasing the efficacy. Jiang et al. [5-7] reported a series of conjugate heat transport investigations for cutting-edge mist-assisted film cooling. They concluded that 13% mist reduces average wall temperature by 20 to 48 K at mid-span [7]. Abdelmaksoud and Wang [8] published a conjugate heat transfer research for turbine blade mist cooling. They discovered that mist-assisted film cooling resulted in a maximum decrease in wall temperature (pressure side) of 250, 340, and 450K for mist concentrations of 10, 15, and 20%. Prior research has primarily focused on flat plate mist-assisted film cooling, with little attention paid towards the curved surfaces. The current idea involves the development of a mist-assisted film cooling technology for turbine blade leading edges.

*Corresponding Author: pallab@iitm.ac.in

2. COMPUTATIONAL METHODOLOGY

2.1 Computational Model

In the current numerical study, the blade's leading edge was assumed to be a semi-circular curved plate (see Fig. 1a) with outer and inner diameters of $16.67d$ and $8.33d$, respectively. For cooling the blade leading edge, five rows of 20^0 compound angled film holes were utilised, one along the stagnation line and the other four at an inclination angle of $\pm 25^0$ and $\pm 50^0$ (see Fig. 1b). The film perforations were set in a staggered pattern with an 8d pitch as shown in Fig. 1c. The diameter and length of the film holes were $d = 0.6$ mm and $12.18d$, respectively. A flat plenum with dimension $5d$ was utilised downstream of the curving plate, and a backside flat end plate with dimensions $1.67d$ was used for the purpose of five impingement holes on the backside of the plate. All impingement holes were positioned in such a way that impingement jets were striking in the centre of two neighbouring stagnation film holes (see Fig. 1d). Only half of the plate was solved using symmetry boundary conditions along plane A-A to reduce computing cost and time.

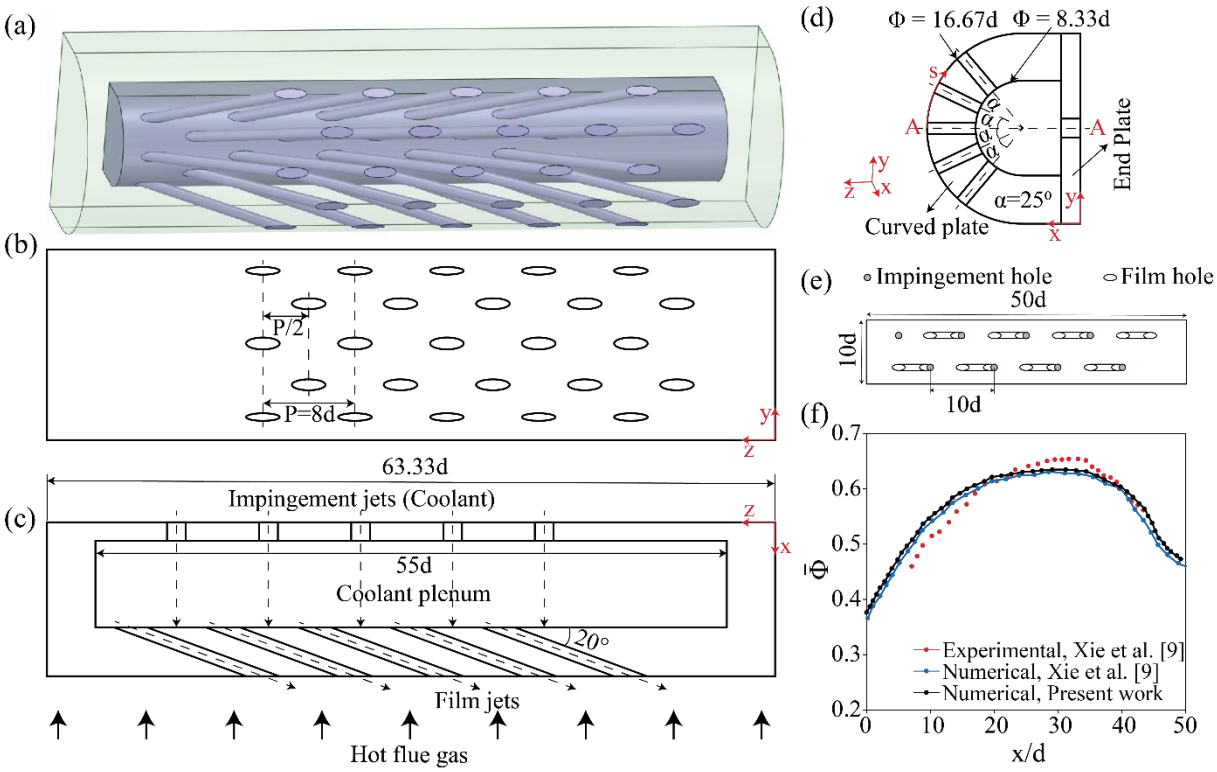

Figure 1: Schematic design of the curved plate (a) 3D leading edge model, (b) y-z plane view of the outer surface of the curved plate and (c) cross-sectional view on symmetry plane (A-A), (d) 2D representation of curved plate on the x-y plane, (e) schematic representation of test plate of Xie et al. [9], and (f) distribution of laterally averaged effectiveness of present numerical work and published data of Xie et al. [9].

2.2 Governing Equations

The current numerical modeling uses the Euler-Lagrangian method to solve the continuous phase (air and vapor) and discrete phase (mist particle). The steady-state Navier-Strokes equations were solved in the continuous phase, and the discrete phase particles were tracked using a continuous flow field. Exchanging mass, momentum, and energy between continuous and discrete phases were used to connect continuous and discrete phase calculations.

2.2.1 Continuous Phase

This section describes the steady-state governing equations for mass [Eq. (1)], momentum [Eq. (2)], and energy equations for fluid [Eq. (3)] and solid [Eq. (4)].

$$\frac{\partial u_i}{\partial x_i} = S_m \tag{1}$$

$$\rho \frac{\partial}{\partial x_j}(u_i u_j) = -\frac{\partial P}{\partial x_i} + \rho\overrightarrow{g_j} + \frac{\partial}{\partial x_j}\left[\mu\left(\frac{\partial u_i}{\partial x_j} + \frac{\partial u_j}{\partial x_i} - \frac{2}{3}\delta_{ij}\frac{\partial u_i}{\partial x_j}\right)\right] + \frac{\partial}{\partial x_j}\left(-\rho\overline{u_i' u_j'}\right) + F_m \tag{2}$$

Here u' is the velocity fluctuating component. According to the Boussinesq hypothesis, turbulent induced stresses $(-\rho\overline{u_i' u_j'})$ can be expressed as below

$-\rho\overline{u_i' u_j'} = \mu_t\left(\frac{\partial u_i}{\partial x_j} + \frac{\partial u_j}{\partial x_i}\right) - \frac{2}{3}\left(\rho k + \mu_t \frac{\partial u_i}{\partial x_j}\right)\delta_{ij}$ and Kronecker delta, $\delta_{ij} = \begin{bmatrix}1, & i = j\\ 0, & i \neq j\end{bmatrix}$.

$$\frac{\partial}{\partial x_i}\left(\rho C_p u_i \mathrm{T}\right) = \frac{\partial}{\partial x_j}\left[k_{eff}\frac{\partial T}{\partial x_i} - \rho C_p \overline{u_i' T'}\right] + \mu\varphi + S_e \tag{3}$$

$$k_s \frac{\partial^2 T}{\partial x_i^2} = 0 \tag{4}$$

Here, $S_m, F_m \; and \; S_e$ are discrete phase calculated source terms. $k_{eff} = k + C_p\mu_t/Pr_t$ is the effective thermal conductivity. Mist particles will evaporate from the discrete phase to the continuous phase. Below is the species transfer equation.

$$\frac{\partial}{\partial x_i}(\rho u_i C_i) = \frac{\partial}{\partial x_i}\left[\rho D_{eff}\frac{\partial C_j}{\partial x_i} - \rho\overline{u_i' C_j'}\right] + S_j$$

In the above equation, C_i is species mass fraction (water vapour) and $D_{eff\,j} = D + \mu_t/Sc_t$ is species effective diffusion coefficient. For Pr_t and Sc_t, constant values of 0.85 and 0.70 were chosen, respectively [10].

2.2.2 Discrete Phase

The Lagrangian method tracks the mist particle in the discrete phase. The air temperature drops due to the evaporation of mist particles in a discrete phase. For the discrete phase, additional equations are solved to include the species transfer. Integrating the force balance on the particle may be used to predict heat and mass transfer for a particle's tracking [10]. It is written as follows in a Lagrangian reference frame:

$$\frac{du_i^p}{dt} = F_D\left(u_i^p - u_i\right) + g\frac{\rho_p - \rho}{\rho_p} + F_p$$

Here, $F_D\left(u_i^p - u_i\right)$ is the drag force per unit particle mass where, u_i^p is the velocity of the droplet and $F_D = \frac{3}{4}\frac{\mu C_D Re_p}{\rho_p d_p^2}$

Where, C_D is the coefficient of drag which varies with Re_p and $Re_p = \frac{\rho d_p |u_p - u|}{\mu}$ is the relative Reynolds number. $C_D = \frac{24}{Re_p}$ for $Re_p \leq 1$ and $C_D = \frac{24}{Re_p}\left(1 + \frac{1}{6}Re_p^{2/3}\right)$ for $1 \leq Re_p \leq 400$.

The energy equation for mist particle is described as

$$m_p C_p \frac{dT_p}{dt} = hA_p\left(T_\infty - T_p\right) + \frac{dm_p}{dt} h_{fg}$$

Here, h_{fg} is the latent heat of vaporization. T_∞ and T_p are bulk air and droplet temperature, respectively. The vaporization rate $\left(dm_p/dt\right)$ is the function of concentration difference.

$$\frac{dm_p}{dt} = -A_p k_c (C_s - C_m)$$

Here, k_c is the mass transfer coefficient. C_s and C_m are the vapou concentrations at the droplet surface and bulk flow, respectively. The evaporation rate may be given as below when the droplet temperature reaches the boiling point.

$$\frac{dm_p}{dt} = -A\left(\frac{\mathrm{k}}{d}\right)\left(2.0 + 0.46 Re_p^{0.5}\right) \ln\left(1 + C_p\left(T_m - T_p\right)/h_{fg}\right)/C_p$$

The stochastic approach was utilized to estimate the turbulence dispersion impact on particle tracking. The particle trajectories are calculated using the instantaneous flow velocity. The source terms $(S_m, F_m \; and \; S_e)$ for continuous phase owing to mass diffusion from discrete to continuous phase, drag force momentum loss, and heat sink are expressed as below [10]

$$S_m = \frac{\Delta m_p}{m_{p,o}} \frac{\dot{m}_{p,o}}{dV} \quad and \quad F_m = \sum\left(\frac{18\mu C_D Re_p}{24\rho_p d_p^2}\left(u_{p,i} - u_i\right)\dot{m}_p \Delta t\right)$$

$$S_e = \frac{1}{dV}\frac{\dot{m}_{p,o}}{m_{p,o}}\left[\left(m_{p,in} - m_{p,out}\right)\left(-H_{lat,ref} + H_{pyrol}\right) - m_{p,out}\int_{T_{ref}}^{T_{p,out}} C_{p_p}\, dT + m_{p,in}\int_{T_{ref}}^{T_{p,in}} C_{p_p} dT\right]$$

2.3 Boundary Conditions and Solver Settings

A commercial finite volume-based software package ANSYS fluent 18.1 was used in this numerical work. The hot flue gas (mainstream) has a constant and uniform velocity of $V_m = 10\, m/s$ and a temperature of $T_m = 353\, K$ were utilised, however for the cooling air ($T_c = 303\, K$), a fixed mass flow rate ($\dot{m}_c = 0.04157\; g/s$) was used to achieve a blowing ratio $M = (\rho_c u_c \,/\, \rho_m u_m) = 1$. The effect of water particles on mist-assisted film cooling was done by adding 2% mist particle (on a mass basis) and droplet size of $d_p = \; 5, 10 \; and \; 15\mu m$. All solid-fluid walls were subjected to the no-slip condition and coupled boundary ($T_f = \; T_s \; and \; k_f \; \partial T_f/\partial x = k_s \; \partial T_s/\partial x$) were utilized for the common interface of two domains. A pressure-based SIMPLE algorithm was utilized in conjunction with a second-order upwind discretization method to couple the pressure and velocity. This study used the two-equation turbulence model ($SST \; k - \omega$ model) with the conservation equations for mass, momentum, and energy. The turbulence model used in this investigation was selected based on available literature and a validation study conducted in this work.

2.4 Validation

Present numerical modelling was validated against the published experimental and computational data of Xie et al. [9]. A flat plate with 10 rows of 30^0. This study employed angled film holes with 4 film holes in each row. The axial and transverse pitch were both $10d$, and the film hole diameter was $d = 4\; mm$ (see Fig. 1e). Case-A of Xie et al. [9], which had a blowing ratio and H/d of 0.9 and 2.5, respectively was considered in this. The other parameters and boundary conditions were set in the same way as in the experiment by Xie et al. [9]. The computational lateral averaged effectiveness trend is the same as that of the experimental data, as shown in Fig. 1f. The present numerical data and previously reported numerical data are in good agreement. The modest variation from experimental values is attributable to the $SST \; k - \omega$ turbulence model under-predicting film cooling and the adiabatic boundary condition at the plate's sidewall.

3. RESULTS AND DISCUSSIONS

The water droplets vaporize before reaching the mainstream, lowering the initial coolant air temperature T_c. As a result, the coolant temperature drops below T_c. To keep the effectiveness value from exceeding one, even for mist-air cooling, the wet-bulb temperature $T_{wet\ bulb}$ was used for calculating the effectiveness $(\Phi = T_m - T_{wall})/(T_m - T_{c,wet\ bulb})$. Figure 2a shows the laterally averaged overall effectiveness distribution along the streamwise direction. Only two-pitch dimensions were taken into account when computing the lateral averaging. It can be seen that adding 2% mist to the coolant increased the effectiveness of the air without changing the trend. The evaporation of mist particles in the coolant air causes this improved cooling effect. Between two consecutive film holes, overall effectiveness decreases then increases slightly near the trailing edge of subsequent film holes. This is owing to the upstream conductive cooling provided by the film jet. It should be noted that the effectiveness does not change substantially in the flat plenum area $(13 \leq \frac{s}{d} \geq 18)$. The effect of droplet sizes was also examined with a fixed mist concentration. As the larger droplet takes longer to evaporate, a modest reduction in cooling performance was found with the droplet size increased. For a droplet size of $d_p = 5\ \mu m$, the maximum improvement in area-weighted averaged effectiveness was ~32%. The surface contours of local adiabatic effectiveness for both air and mist cases are presented in Fig. 2b. In comparison to the air case, mist case effectiveness is substantially higher near the film hole outlet, and the mist case also has a larger film covering area.

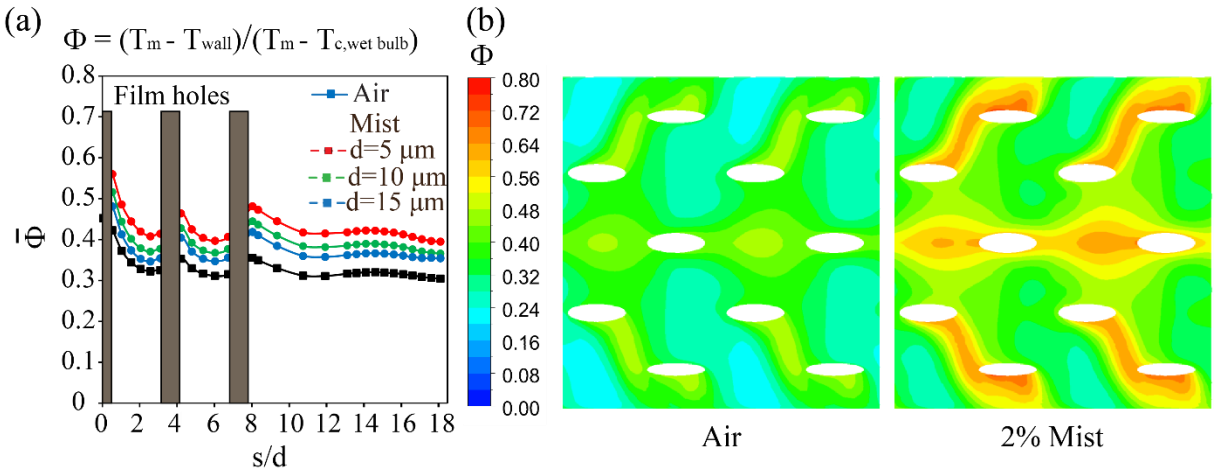

Figure 2: Distribution of overall film cooling effectiveness for $M = 1$ (a) laterally averaged effectiveness along the streamwise direction, and (b) local effectiveness contours on the outer surface of the curved plate for droplets diameter $d_p = 5\ \mu m$.

Figures 3a and b show the distribution of local temperature contours superimposed with velocity. The temperature inside the coolant plenum appears to be dropping below the coolant temperature at that inlet, which is 303 K. This is due to the mist particle evaporating, which serves as a heat sink. For air and mist-assisted film cooling, the coolant temperature at the film exit is $\sim 320\ K$ and $\sim 310\ K$, respectively. As a result, as compared to the only air case, this low-temperature coolant will keep the outside target surface and blade material at lower temperatures. The particle tracking of mist particles is demonstrated in Fig. 3c. Droplet size was noticeably reduced from the coolant inlet to the computational domain's outlet, and droplets were not entirely evaporating at the outlet, indicating that the travel distance was insufficient. Droplets with a diameter of $d_p = 5\ \mu m$ may be seen at the coolant jet's inlet. As it enters the coolant plenum, it begins to evaporate, causing the size of the droplets to decrease as it flows towards the flow domain's outlet.

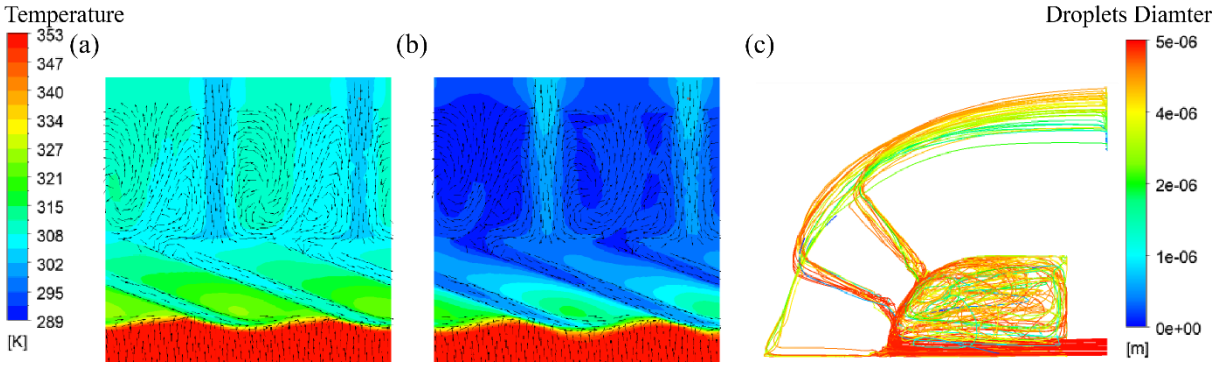

Figure 3: Distribution of temperature contour with velocity vectors at the symmetry plane (a) air film cooling, (b) mist-assisted film cooling and (c) particle tracking of water droplets for mist-assisted film cooling for droplets diameter $d_p = 5\ \mu m$.

4. CONCLUSIONS

A numerical study has been performed to study the effect of the addition of mist droplets in coolant air on film cooling performance. Compared to an air case, a larger film coverage area with improved cooling performance was observed in the mist case. The area-weighted averaged effectiveness was also increased by $\sim 32\%$ for a droplet size of $d_p = 5\ \mu m$. The mist-assisted film cooling area was also found to diminish with an increase in droplet size since larger droplets take longer to evaporate and travel far compared to smaller droplets. Thus, mist-assisted film cooling can be used for better thermal management of turbine components.

REFERENCES

[1]. A. K. Jaiswal, P. S. Mahapatra, and B. V. S. S. S. Prasad, Effect of microchannel on combined impingement and film cooling of a concave surface. *International Communications in Heat and Mass Transfer*, **126** (2021), 105441.

[2]. N. V. Nirmalan, J. A. Weaver, and L. D. Hylton, An experimental study of turbine vane heat transfer with water–air cooling. *Journal of Turbomachinery*, **120** (1998), 50–60.

[3]. X. Li, and T. Wang, Simulation of film cooling enhancement with mist injection. *Journal of Heat Transfer*, **128** (2006), 509–519.

[4]. L. Zhao, and T. Wang, An experimental study of mist/air film cooling on a flat plate with application to gas turbine airfoils—Part I: heat transfer. *Journal of Turbomachinery*, **136** (2014).

[5]. Y. Jiang, Q. Zheng, P. Dong, G. Yue, and J. Gao, Numerical simulation on turbine blade leading-edge high-efficiency film cooling by the application of water mist. *Numerical Heat Transfer, Part A: Applications*, **66** (2014), 1341–1364.

[6]. Y. Jiang, Q. Zheng, P. Dong, H. Zhang, and F. Yu, Research on heavy duty gas turbine vane high efficiency cooling performance considering coolant phase transfer. *Applied Thermal Engineering*, **73** (2014), 1177–1193.

[7]. Y. Jiang, Q. Zheng, P. Dong, J. Yao, H. Zhang and J. Gao, Conjugate heat transfer analysis of leading edge and downstream mist–air film cooling on turbine vane. *International Journal of Heat and Mass Transfer*, **90** (2015), 613-626.

[8]. R. Abdelmaksoud, and T. Wang, Simulation of air/mist cooling in a conjugate, 3-d gas turbine vane with internal passage and external film cooling. *International Journal of Heat and Mass Transfer*, **160** (2020), 120197.

[9]. G. Xie, C. L. Liu, L. Ye, R. Wang, J. Niu, and Y. Zhai, Effects of impingement gap and hole arrangement on overall cooling effectiveness for impingement/effusion cooling. *International Journal of Heat and Mass Transfer*, **152** (2020), 119449.

[10]. Fluent, FLUENT 17.2 User's Guide FLUENT, Inc. NH, Lebanon, (2017).